

Marquette University

e-Publications@Marquette

Physics Faculty Research and Publications

Physics, Department of

9-2006

Mechanistic Studies on the Mononuclear Zn^{II}-Containing Metallo- β -lactamase ImiS from *Aeromonas sobria*

Narayan Sharma

Miami University - Oxford

Christine E. Hajdin

Miami University - Oxford

Sowmya Chandrasekar

Miami University - Oxford

Brian Bennett

Marquette University, brian.bennett@marquette.edu

Ke-Wu Yang

Miami University - Oxford

See next page for additional authors

Follow this and additional works at: https://epublications.marquette.edu/physics_fac



Part of the [Physics Commons](#)

Recommended Citation

Sharma, Narayan; Hajdin, Christine E.; Chandrasekar, Sowmya; Bennett, Brian; Yang, Ke-Wu; and Crowder, Michael W., "Mechanistic Studies on the Mononuclear Zn^{II}-Containing Metallo- β -lactamase ImiS from *Aeromonas sobria*" (2006). *Physics Faculty Research and Publications*. 33.
https://epublications.marquette.edu/physics_fac/33

Authors

Narayan Sharma, Christine E. Hajdin, Sowmya Chandrasekar, Brian Bennett, Ke-Wu Yang, and Michael W. Crowder

Marquette University

e-Publications@Marquette

Physics Faculty Research and Publications/College of Arts and Sciences

This paper is NOT THE PUBLISHED VERSION; but the author's final, peer-reviewed manuscript. The published version may be accessed by following the link in the citation below.

Biochemistry, Vol. 45, No. 35 (1 September 2006): 10729–10738. [DOI](#). This article is © American Chemical Society Publications and permission has been granted for this version to appear in [e-Publications@Marquette](#). American Chemical Society Publications does not grant permission for this article to be further copied/distributed or hosted elsewhere without the express permission from American Chemical Society Publications.

Mechanistic Studies on the Mononuclear Zn^{II}-Containing Metallo-β-lactamase ImiS from *Aeromonas sobria*

Narayan P. Sharma

Department of Chemistry and Biochemistry, Miami University, Oxford, Ohio

Christine Hajdin

Department of Chemistry and Biochemistry, Miami University, Oxford, Ohio

Sowmya Chandrasekar

Department of Chemistry and Biochemistry, Miami University, Oxford, Ohio

Brian Bennett

National Biomedical EPR Center, Department of Biophysics, Medical College of Wisconsin, Milwaukee, Wisconsin

Ke-Wu Yang

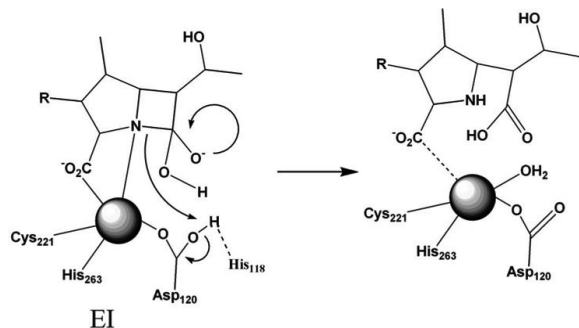
Department of Chemistry and Biochemistry, Miami University, Oxford, Ohio

Michael W. Crowder

SUBJECTS:

Peptides and proteins, Reaction mechanisms, Fluorescence

Abstract



In an effort to understand the reaction mechanism of a B2 metallo-β-lactamase, steady-state and pre-steady-state kinetic and rapid freeze quench electron paramagnetic resonance (EPR) studies were conducted on ImiS and its reaction with imipenem and meropenem. pH dependence studies revealed no inflection points in the pH range of 5.0–8.5, while proton inventories demonstrated at least 1 rate-limiting proton transfer. Site-directed mutagenesis studies revealed that Lys224 plays a catalytic role in ImiS, while the side chain of Asn233 does not play a role in binding or catalysis. Stopped-flow fluorescence studies on ImiS, which monitor changes in tryptophan fluorescence on the enzyme, and its reaction with imipenem and meropenem revealed biphasic fluorescence time courses with a rate of fluorescence loss of 160 s^{-1} and a slower rate of fluorescence regain of 98 s^{-1} . Stopped-flow UV-vis studies, which monitor the concentration of substrate, revealed a rapid loss in absorbance during catalysis with a rate of 97 s^{-1} . These results suggest that the rate-limiting step in the reaction catalyzed by ImiS is C–N bond cleavage. Rapid freeze quench EPR studies on Co^{II}-substituted ImiS demonstrated the appearance of a rhombic signal after 10 ms that is assigned to a reaction intermediate that has a five-coordinate metal center. A distinct product (EP) complex was also observed and began to appear in 18–19 ms. When these results are taken together, they allow for a reaction mechanism to be offered for the B2 metallo-β-lactamases and demonstrate that the mono- and dinuclear Zn^{II}-containing enzymes share a common rate-limiting step, which is C–N bond cleavage.

Bacterial resistance to antibiotics is a growing clinical concern (1, 2). Zn^{II}-containing β-lactamases (metallo-β-lactamases, MβLs)¹ contain 1–2 mol of Zn^{II}/mol of enzyme, hydrolyze all known cephalosporins, carbapenems, and penicillins, are not inhibited by clavulanic acid and other classical β-lactamase inhibitors, and have no known clinically useful inhibitor toward them (3, 4). Previous studies have shown that there is significant structural and mechanistic diversity among the MβLs, leading to the grouping of the enzymes into three distinct subclasses: B1, B2, and B3 (5, 6). Sequence identity ranges from 25–40% between members in one subclass and from 10–20% between members in different subclasses. Subclass B1 enzymes have been found in strains of *Bacillus*, *Bacteroides*, *Pseudomonas*, *Serratia*, and *Chryseobacterium*, and subclass B3 enzymes have been found in strains of *Stenotrophomonas*, *Legionella*, *Fluoribacter*, *Janthinobacterium*, and *Caulobacter* (3, 4). Enzymes from the B1 and B3 subclasses have broad substrate profiles and require two Zn^{II} ions for maximal enzymatic activity (3). In contrast, subclass B2 enzymes have a relatively narrow substrate profile, hydrolyzing

carbapenems almost exclusively (3), and exhibit maximal activity when bound to only 1 Zn^{II} (7). In fact, the binding of a second Zn^{II} ion is inhibitory (7). These carbapenemases are produced by various species of *Aeromonas*. Aeromonads are enteric, anaerobic, Gram-negative pathogens that cause a range of symptoms from mild diarrhea to acute gastroenteritis in humans (8), and *Aeromonas* species have been found in wound infections (9). One alarming characteristic of Aeromonads is that they are waterborne and typically are present in purified, drinking water (10). To date, there is no crystal structure available for ImiS, but the crystal structure of another subclass B2 enzyme, CphA from *Aeromonas hydrophila*, has been recently reported (11). This structure showed Zn^{II} bound to His263, Cys221, Asp120, and a water; this site is the consensus Zn₂ site in MβLs (3). Recent spectroscopic studies have demonstrated that Zn^{II}/Co^{II} preferentially binds to this same site in ImiS (12). Previous biochemical, kinetic, and inhibition studies have suggested significant structural and mechanistic differences among the different group B β-lactamases (3, 4, 13). These results suggest that one inhibitor may not be effective in treating all infections caused by bacteria that produce a MβL. Toney and Moloughney recently reviewed the literature on inhibitors of MβLs (13), and most of these inhibitors are effective against only one or two of the enzymes. This is not surprising because, with few exceptions (14–16), the design of most of the inhibitors was guided by studies on only one enzyme. To address this problem, we are currently characterizing a MβL from each of the group B subclasses (CcrA, ImiS, and L1) in an effort to identify common structural/mechanistic properties of the enzymes toward which a single inhibitor can be designed. While extensive mechanistic studies have been reported on B1 and B3 MβLs (17–24), there is little known about the mechanism of a B2 MβL. Herein, we describe the first detailed mechanistic studies on a B2 MβL, specifically ImiS from *Aeromonas veronii* *bv. sobria*.

Experimental Procedures

Preparation of ImiS Samples.

Recombinant ImiS was prepared as described previously (25). Briefly, the overexpression plasmid, pET26b-ImiS, was used to transform BL21(DE3) *Escherichia coli* cells. A 10 mL overnight culture of these cells in Luria–Bertani (LB) medium was used to inoculate 4 × 1 L of LB medium containing 25 μg/mL kanamycin and 29 μg/mL ZnSO₄·7H₂O. The cells were allowed to grow at 37 °C with shaking until the cells reached an optical density at 600 nm of 0.6–0.8. Protein production was induced with 1 mM isopropyl-β-d-thiogalactopyranoside (IPTG), and the cells were shaken at 37 °C for 3 h. The cells were collected by centrifugation (15 min at 7000g) and resuspended in 30 mL of 50 mM tris(hydroxymethyl)aminomethane (Tris) at pH 7.0 containing 500 mM NaCl. The cells were ruptured by two passages through a French press at 16 000 lb/in., and the cell debris was separated by centrifugation (30 min at 25000g). The cleared supernatant was dialyzed versus 2 L of 50 mM Tris at pH 7.0 overnight at 4 °C, centrifuged to remove insoluble matter, and loaded onto a SP-Sepharose column (1.5 × 12 cm with a 25 mL bed volume) that was equilibrated with 50 mM Tris at pH 7.0. Bound proteins were eluted with a 0–500 mM NaCl gradient in 50 mM Tris at pH 7.0 and 2 mL/min. Fractions (8 mL) containing ImiS were pooled and concentrated with an Amicon ultrafiltration cell equipped with a YM-10 membrane. Protein purity was ascertained by sodium dodecyl sulfate–polyacrylamide gel electrophoresis (SDS–PAGE). ImiS concentrations were determined using Beer's law and an extinction coefficient of 37 250 M⁻¹ cm⁻¹ (25). Co^{II}-substituted ImiS was prepared as previously described (12).

Substrate Inhibition Studies.

Substrate inhibition studies were carried out on recombinant ImiS using imipenem or meropenem as the substrate. Assays were conducted at 25 °C in 50 mM Tris at pH 7.0 on an HP 5480A diode array UV–vis spectrophotometer. Initial velocity versus imipenem concentration data were plotted and fitted with Michaelis–Menten equations assuming different modes of substrate inhibition (26). Imipenem and meropenem were gifts from Merck and Co. (Rahway, NJ) and Zeneca Pharmaceuticals (Wilmington, DE), respectively.

Product Studies.

Hydrolyzed products of imipenem were prepared by incubating 8 mM imipenem in 50 mM Tris at pH 7.0 with either 190 μ M ImiS or 100 μ M L1 (27), and the reactions were incubated on ice for 2 h. The enzymes were removed by using ultrafiltration (Centricon-10), and the resulting product containing solutions were analyzed at 280 and 300 nm using UV-vis spectrophotometry to determine whether the solutions contained any protein or unhydrolyzed imipenem. The solutions were then flash-frozen in liquid nitrogen and lyophilized overnight. The products were analyzed with ^1H nuclear magnetic resonance (NMR) spectroscopy (Bruker 500 MHz) or by liquid chromatography-mass spectrometry (LC-MS) (Bruker Esquire, ESI). The lyophilized products were then dissolved in 50 mM Tris at pH 7.0 and used in product inhibition studies with L1 (nitrocefin as the substrate) and ImiS (imipenem as the substrate).

pH Dependence Studies.

pH dependence studies were performed on recombinant ImiS over the pH range of 5.0–8.5 using a multicomponent buffer, MTEN. MTEN (25 mM MES, 25 mM Tris, 25 mM ethanolamine, and 100 mM NaCl) was used to minimize the effects of using different buffers over wide ranges of pH, and the NaCl was included to normalize the ionic strength effects in the buffer (28). The pH of the buffers was ascertained by using a pH-meter. Steady-state kinetic assays were conducted at 25 °C in 50 mM Tris buffer at pH 7.0 on a HP 5480 diode array UV-vis spectrophotometer. Steady-state kinetic constants, K_M and k_{cat} , were determined by fitting initial velocity versus substrate concentration data directly to the Michaelis-Menten equation using Igor Pro version 4.0.5.1 (Wavemetrics). The pH dependence data were fitted with Leonara (29); however, no pK_a values above 5.5 or below 8 were revealed with this software.

Proton Inventories.

Proton inventories were performed with ImiS in MTEN buffer at pH/pD 7.0 using imipenem as the substrate. Enzyme and substrate were incubated in the D_2O -containing buffer for 30 min to allow for full proton-deuteron equilibration. Data were collected in buffers containing 0, 25, 50, 75, and 100% D_2O [mole fraction of D_2O (n) = 0, 0.25, 0.5, 0.75, and 1.0]. The steady-state kinetic constant, k_{cat} , was obtained as described above. The resulting kinetic constants were plotted versus their mole fraction D_2O and fitted to the Gross-Butler equation for one ($k_{cat\ 0}[1 - n + (n(k^D/k^H))]$), two ($k_{cat\ 0}[1 - n + (n(k^D/k^H))][1 - n + (n(k^D/k^H))]$), and multiple ($k_{cat\ 0}[(k^D/k^H)^n]$) protons in flight models (30, 31).

Generation and Characterization of K224T and N233S Mutants.

Using the PAGE-purified oligonucleotides primers and the overexpression plasmid for ImiS (pET26b-ImiS) as the template, ImiS mutants were generated using the Quikchange site-directed mutagenesis kit according to the instructions of the manufacturer. The primers used for the mutagenesis studies were K224T forward, CTTTATggCAACTgCATCCTCACCgAGAAGCTgggCAACCTgAgCTTTgCC; K224T reverse, ggCAAAGCTCAGgTTgCCCAGCTTCTCggTgAggATgCAGTTgCCATAAAg; N223S forward, gCCTTCACATCggCAAAGCTCAGgCTgCCCAGCTTCTCCTTgAggAT; N223S reverse, ATCCTCAAggAgAAgCTgggCAGCCTgAgCTTTgCCgATgTgAAggC. DNA sequencing of the mutated *imiS* genes using T7 forward (TAATACgACTCACTATAgg) and T7 reverse (CgATCAATAACGAgTCgCC) as the primers was used to confirm the presence of the mutation and that no other unintended mutations were present in the genes. These DNA sequences were analyzed on the Perkin-Elmer ABI 3100 genetic analyzer.

To test for the overexpression of mutants, the mutant plasmids were transformed into *E. coli* BL21(DE3) cells and small-scale cell cultures were used (32). Large-scale 4 L preparations were performed using the protocol described above for wild-type ImiS. Zn^{II} -loaded samples of ImiS and ImiS mutants were made 100 μ M in Zn^{II} and incubated for 30 min on ice. The samples were then dialyzed versus 3×1 L of metal-free, 50 mM Tris at pH 7.0

and 4 °C over a 6 h time period to remove any unbound Zn^{II}. These Zn^{II}-loaded samples of ImiS and ImiS mutants were diluted to a final enzyme concentration of 5–10 μM. The metal content of these samples was determined using a Varian Liberty 2 inductively coupled plasma spectrometer with atomic emission spectroscopy detection (ICP–AES). The final dialysis buffer was used as a blank. Calibration curves for all metals tested were based on at least three concentration replicates, and all calibration curves had correlation coefficients of 0.9950 or better. Emission lines were monitored at 213.856, 238.892, 324.754, 259.940, 257.610, and 231.604 nm, with the most intense emissions for zinc, cobalt, copper, iron, manganese, and nickel, respectively. Errors in metal content were reported as standard deviations (σ_{n-1}) of replicate samples.

Zn^{II}-loaded ImiS and ImiS mutants were dialyzed versus 3 × 2 L of 5 mM phosphate at pH 7.0 over 6 h. The samples were then diluted with the same buffer to a final concentration of approximately 75 μg/mL. Circular dichroism (CD) spectra were obtained on a JASCO J-810 CD spectropolarimeter, operating at 25 °C. CD spectra were analyzed for secondary structural content using the CONTIN simulation program at DICHROWEB (<http://www.crysl.bbk.ac.uk/cdweb/html/home.html>) (33, 34).

Zn^{II}-loaded ImiS and ImiS mutants were diluted with metal-free, 50 mM Tris at pH 7.0 to a final concentration of 2 μM. Fluorescence spectra were obtained at 25 °C using an excitation wavelength of 295 nm on a Perkin-Elmer LS55 luminescence spectrophotometer.

Stopped-Flow Kinetic Studies.

Hydrolysis of imipenem (10–350 μM) by ImiS (120 μM) in 50 mM Tris buffer at pH 7.0 and 2 °C was followed by electronic absorption at 300 nm and by 280 nm excited fluorescence emission at ≥320 nm (320 nm cutoff filter) on an Applied Photophysics SX18MV spectrophotometer. Time-dependent electronic absorption spectra of Co^{II}-substituted ImiS (500 μM) were collected using a photodiode array (PD.1, Applied Photophysics) upon the reaction with 500 μM imipenem at 2 °C. Kinetic data were fitted to either single- or double-exponential equations using KinTekSim version 3.20 software (<http://www.kintek-corp.com/>). Stopped-flow fluorescence data were also globally fitted using Applied Photophysics PC ProK global analysis software.

Kinetic Simulations.

Kinetic simulations were conducted using KINSIM (35). The values for flux and integral tolerances were left as the default values of 0.02 and 1×10^{-6} , respectively.

Rapid Freeze Quench (RFQ) Electron Paramagnetic Resonance (EPR) Spectra.

Samples for RFQ–EPR studies were generated using a modified Update Instruments (Madison, WI) RFQ system (21). The RFQ system was calibrated by comparing the development of a low-spin Fe^{III} EPR signal and the disappearance of a high-spin Fe^{III} EPR signal with the associated optical changes at 636 nm using stopped-flow spectrophotometry, upon mixing myoglobin with an excess of sodium azide. The shortest, total effective reaction time that could be achieved with the RFQ system was 10 ms. The initial concentrations of Co^{II}-substituted ImiS and imipenem were 1 and 5 mM, respectively. EPR spectra were recorded using a Bruker EleXsys E500 EPR spectrometer equipped with an Oxford Instruments ITC4 temperature controller and an ESR-900 helium flow cryostat. Spectra were recorded at 12 K with 1 mW microwave power. A Bruker ER-4116DM cavity was used, with a resonant frequency of 9.63 GHz (in perpendicular mode), and 10 G (1 mT) field modulation at 100 kHz was employed. Computer simulations of EPR spectra were carried out using the matrix diagonalization program XSophe [Bruker Biopsin GmbH] (36), assuming a spin Hamiltonian $H = \beta gBS + SDS + SAI$, where $S = 3/2$ and $D > 0$ corresponds to an $M_S = |\pm 1/2\rangle$ ground-state Kramers' doublet. For Co^{II}, generally $D \gg \beta gBS$ and the spectrum is therefore insensitive to the precise value of D (37); in this work, the arbitrary value $D = 50 \text{ cm}^{-1}$ was used. The g tensor was assumed to have at least axial symmetry because this allows for a unique solution to the spin Hamiltonian in terms of the real g values, g_z and $g_{x,y}$ (or g_{\parallel} and g_{\perp}), and the rhombic

distortion of the axial zero-field splitting, E/D (37). The relationship between the resonance positions, $g_{\text{eff}(x,y,z)}$, and these parameters are described in detail elsewhere (38, 39). Line widths were simulated using a single-strain parameter for each of the principal orientations. Where simulations of spectra are shown that contain more than one species, spectra that could be well-simulated assuming a single set of spin Hamiltonian parameters were used as basis spectra and linear combinations of two (and no more than two) basis spectra were used to model the spectra collected after reaction times, intermediate between those after which the basis spectra were recorded. Contributions of the individual species are estimated as $\pm 5\%$ of the total spins.

Results

Substrate Inhibition.

Many enzymes conform to Michaelis–Menten kinetics over a limited range of substrate concentrations but deviate at higher substrate concentrations (40). Steady-state kinetic studies with ImiS and using imipenem or meropenem resulted in Michaelis–Menten plots that indicate significant substrate inhibition (Figure 1). Several substrate inhibition models [competitive, noncompetitive, etc. (26)] were tested to fit the observed steady-state kinetic data, and a model defined by uncompetitive substrate inhibition was the model that best-fitted the data (line in Figure 1).

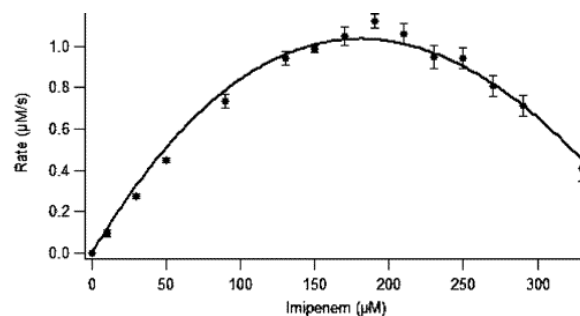


Figure 1 Michaelis–Menten plot of imipenem hydrolysis by ImiS in 50 mM Tris at pH 7.0 and 25 °C. The data were fitted to a Michaelis–Menten equation with uncompetitive substrate inhibition (26).

Product Inhibition Studies.

The recent crystal structure of CphA showed a unique bicyclic “intermediate” in the active site of the enzyme that is formed by the attack of the invariant hydroxyl group of the 6′ substituent of biapenem (and other carbapenems) on the 3′ carbon of the five-membered ring (11). Garau et al. argued that the formation of the second ring in the product occurs after C–N bond cleavage (11). To ascertain whether this bicyclic, hydrolyzed carbapenem is catalytically competent, we hydrolyzed imipenem with ImiS and with L1. L1 and ImiS were removed from the solutions by ultrafiltration, and the products were analyzed with ^1H NMR spectroscopy and LC–MS. There were no differences in the mass spectra or the NMR spectra of the two products. Neither product absorbed in the UV–vis region about 280 nm.

Therefore, the ImiS- and L1-generated products were used in product inhibition studies. The ImiS-generated product inhibited ImiS with a K_i of $53 \pm 5 \mu\text{M}$ and inhibited L1 with a K_i of $615 \pm 50 \mu\text{M}$. The L1-generated product inhibited ImiS with a K_i of $4 \pm 1 \text{ mM}$ and inhibited L1 with a K_i of $2 \pm 1 \text{ mM}$. Clearly, the ImiS-generated product is distinct from the L1-generated product.

pH Dependence Studies.

pH dependence kinetic studies can be used to probe for groups with ionizable protons associated on the free enzyme, free substrate, or enzyme–substrate complex (40). In pH dependence studies on Zn^{II} -containing ImiS, a relatively narrow pH range of 5.0–8.5 was used because ImiS precipitated at pH values below 5.0 and above 8.5.

A multicomponent buffer, MTEN (28), was used to minimize buffer and ionic strength effects. The $\log k_{\text{cat}}$ and $\log(k_{\text{cat}}/K_M)$ versus pH plots (Figure 2) for hydrolysis of imipenem by Zn^{II}-containing ImiS were fitted with Leonara (29); however, no pK_a values above 5.5 or below 8.0 were revealed. Similar results have been reported for the dinuclear Zn^{II}-containing β -lactamases L1 and CcrA (18, 41). pH dependence plots for Co^{II}-substituted ImiS with imipenem also did not reveal any inflection points (data not shown).

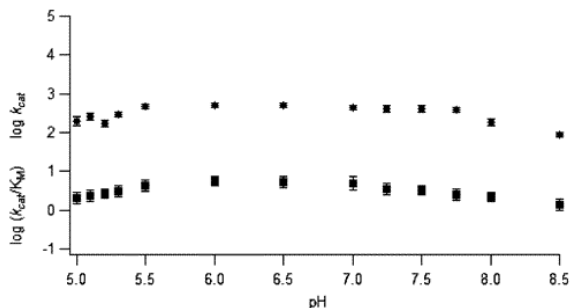


Figure 2 pH dependence plots of $\log k_{\text{cat}}$ (●) and $\log k_{\text{cat}}/K_M$ (■) for the hydrolysis of imipenem by ImiS in MTEN buffer. The data points represent average values from at least three trials. Error bars represent the standard deviation of multiple trials.

Solvent Isotope Studies.

Solvent isotope studies have been extensively used in the literature to probe reaction mechanisms of enzymes, specifically to identify any rate-limiting proton transfers (31). The hydrolysis of imipenem by ImiS yielded a solvent isotope effect (k^H/k^D) of 1.7 ± 0.2 , suggesting a proton transfer during a nucleophilic reaction. A proton inventory of ImiS yielded a k_{cat} versus mole fraction of D₂O that was best-fitted to a multiple proton in flight model (Figure 3); however, we cannot unambiguously rule out the one or two proton in flight models (30). Similar proton inventories have been reported for dinuclear Zn^{II}-containing L1 and CcrA (28, 41).

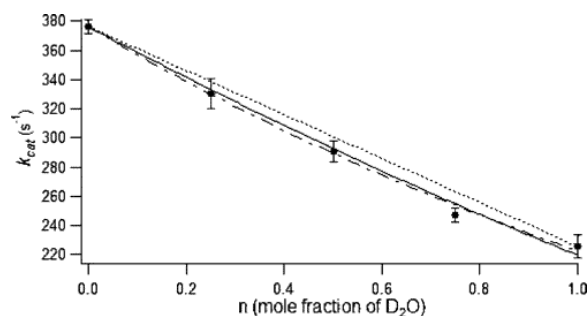


Figure 3 Proton inventory of imipenem hydrolysis by ImiS. Data points represent averages of at least three trials, and error bars are standard deviations. The data were fitted to single proton (···), two proton (—), and multiple proton in flight (---) models (30).

K224T and N233S Mutants of ImiS.

A lysine is located at position 224 in all sequenced M β Ls except in L1 from *Stenotrophomonas maltophilia* (6). Lys224 has been proposed to be involved in substrate binding via electrostatic interactions with the invariant carboxylate group of the β -lactam-containing antibiotics (11, 42, 43). To test this hypothesis, Lys224 was mutated to a threonine using site-directed mutagenesis. Bordo and Argos have reported that threonine is the “safest” substitution in mutagenesis studies for exposed lysines (44). Small-scale cultures were used to show that the K224T mutant could be overexpressed and purified at levels comparable to wild-type ImiS. CD and

fluorescence spectra of the K224T mutant were similar to those of wild-type ImiS (data not shown), suggesting that the point mutation does not result in large structural changes in the enzyme.

Metal analyses on as-isolated and Zn^{II}-loaded K224T demonstrated that the mutant binds 0.80 and 0.78 equiv of Zn^{II}, respectively, which is similar to the metal content of wild-type ImiS (Table 1). Steady-state kinetics revealed that this mutant exhibited a 16-fold drop in k_{cat} and a 4-fold increase in K_M when using imipenem as a substrate (Table 1). In studies using meropenem as the substrate, the K224T mutant exhibited no change in K_M and a 740-fold decrease in k_{cat} (Table 1).

Table 1: Steady-State Kinetic Constants and Metal Content of ImiS Mutants^a

enzyme	imipenem k_{cat} t (s^{-1})	imipenem K_M (μM)	meropenem k_{cat} t (s^{-1})	meropenem K_M (μM)	Zn ^{II} equiv as-isolated	Zn ^{II} equiv Zn ^{II} -loaded ^b
wild type	350 ± 15	100 ± 10	296 ± 20	308 ± 55	0.90 ± 0.06	0.85 ± 0.06
K224T	17 ± 3	208 ± 90	0.67 ± 0.07	136 ± 30	0.80 ± 0.07	0.78 ± 0.15
N233S	303 ± 27	109 ± 22	270 ± 28	151 ± 33	0.77 ± 0.08	0.90 ± 0.08

^a Steady-state kinetic constants and metal content were determined on at least three different preparations of the enzymes. Steady-state kinetic studies were conducted in 50 mM Tris at pH 7.0 and 25 °C. ^b Zn^{II}-loaded samples were prepared by incubating the as-isolated enzymes with 100 μM Zn^{II} for 30 min and dialyzed 3 times versus 1 L of 50 mM Tris at pH 7.0 for 2 h each.

An asparagine is located at position 233 in all M β Ls except L1 from *S. maltophilia* (subclass B3) (45), BlaB (subclass B1) (46), and IND-1 from *Chryseobacterium* species (subclass B1) (47). The N233S mutant could be overexpressed and purified at levels comparable to that of wild-type ImiS. This mutant also exhibited CD and fluorescence spectra similar to those of wild-type ImiS (25), suggesting that the point mutation did not cause a change in the structure of the enzyme. Metal analyses revealed that as-isolated and Zn^{II}-loaded N233S bound 0.77 and 0.99 equiv of Zn^{II}, respectively (Table 1). Steady-state kinetics revealed that the N233S mutant exhibited steady-state kinetic constants similar to those of wild-type ImiS (Table 1).

Stopped-Flow Kinetic Studies.

In initial stopped-flow UV-vis studies, we reacted Co^{II}-substituted ImiS with imipenem and we monitored the reaction using diode array detection, particularly in the 500–650 nm region of the spectra, in an effort to probe the ligand field transitions of high-spin Co^{II} during the course of the reaction. In all of the experiments that we conducted, there were no observable changes in the intensities of the ligand field bands. Therefore, we chose to monitor the change in absorbance of the substrate during the course of the reaction. The rate of imipenem hydrolysis, monitored by stopped-flow spectrophotometry (Figure 4), was a complex function of the concentration of imipenem and exhibited uncompetitive substrate inhibition (Figure 1). A single-exponential fit to the single-turnover progress curve with 100 μM imipenem returned a turnover rate of 97 s^{-1} at 2 °C.

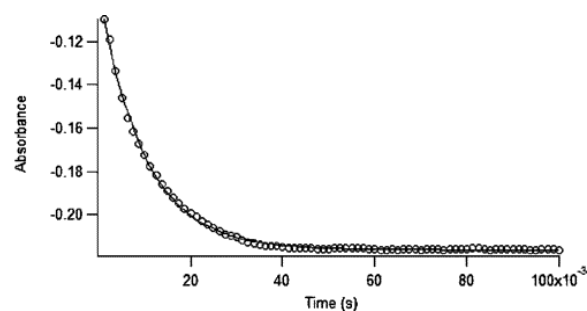


Figure 4 Stopped-flow UV-vis data (data points) collected at 300 nm for the reaction of 120 μM ImiS with 100 μM imipenem in 50 mM Tris buffer at pH 7.0 and 2 $^{\circ}\text{C}$. The solid line is the simulated progress curve generated by KINSIM when using the kinetic mechanism in Scheme 1 and the rate constants in Table 2.

Single-turnover (100 μM imipenem/meropenem and 120 μM ImiS) reactions were also probed with stopped-flow fluorescence studies, which monitor tryptophan fluorescence of the enzyme during catalysis. The resulting stopped-flow fluorescence time courses were biphasic and showed a substantial quenching of fluorescence over the first 10 ms of the reaction, followed by a relatively slow regain to baseline levels over the subsequent 45 ms of the reaction. The stopped-flow fluorescence data were fitted with a double-exponential equation, which yielded a rate of $160 \pm 4 \text{ s}^{-1}$ for the initial quenching phase and a rate of $98 \pm 1 \text{ s}^{-1}$ for the slower fluorescence regain phase (Figure 5). Additional experiments were conducted at higher substrate and lower ImiS concentrations. However, as with the stopped-flow UV-vis studies, the rates of fluorescence quench and regain were lower at substrate concentrations $> 200 \mu\text{M}$.

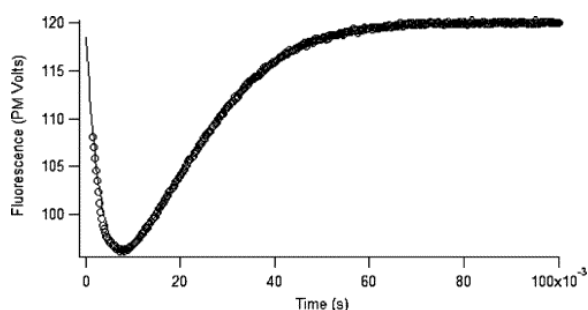
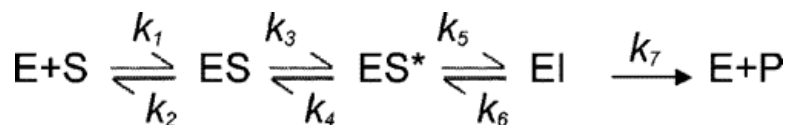


Figure 5 Stopped-flow fluorescence data (data points) of 120 μM ImiS reacted with 100 μM imipenem in 50 mM Tris at pH 7.0 and 2 $^{\circ}\text{C}$. The data points show time dependence of the fluorescence emission at 320 nm after excitation at 280 nm. The solid line is the simulated progress curve generated by KINSIM when using the kinetic mechanism in Scheme 1 and the rate constants in Table 2.

Global Fittings and KINSIM Simulations.

Using previously reported kinetic mechanisms (17, 40, 48) and PC ProK global-fitting software, the stopped-flow fluorescence data were fitted. The simple Michaelis-Menten mechanism was tested first, and more complicated mechanisms were subsequently tested. The simplest mechanism that sufficiently fitted the data is shown in Scheme 1; this mechanism was previously proposed for dinuclear Zn^{II} -containing M β L L1 from *S. maltophilia* when reacted with meropenem or cefaclor (48) (Table 2). Using the rate constants (Table 2), the mechanism in Scheme 1, and KINSIM (35), we could suitably simulate the stopped-flow fluorescence and UV-vis data (lines in Figures 4 and 5). The global fittings and kinetic simulations show that the rate constants determined with single-turnover experiments are equal to k_5 and k_7 . This scenario supports our analyses that the second and third steps (k_4 and k_6 , Scheme 1) of the mechanism are essentially irreversible.



Scheme 1

Table 2: Results of Global-Fitting Analysis of Stopped-Flow Fluorescence Data to Scheme 1^a

parameter	fitted rate
$k_1 (\text{M}^{-1} \text{s}^{-1})$	$1.0 \times 10^8 \pm 1.0 \times 10^3$

k_2 (s ⁻¹)	$1.0 \times 10^4 \pm 1.0 \times 10^{-3}$
k_3 (s ⁻¹)	990 ± 1
k_4 (s ⁻¹)	$2.4 \times 10^{-4} \pm 8.6 \times 10^{-7}$
k_5 (s ⁻¹)	163 ± 1
k_6 (s ⁻¹)	$4.0 \times 10^{-3} \pm 1.7 \times 10^{-6}$
k_7 (s ⁻¹)	98 ± 1

^a Substrate used in the stopped-flow studies was imipenem. Data were fitted with Applied Photophysics PC ProK global-fitting software using the mechanism in Scheme 1. The reported uncertainties represent standard errors as determined by the ProK software (nonlinear Marquardt–Levenberg algorithm).

The values obtained from the global fittings (Table 2) were used to calculate steady-state parameters according to $k_{\text{cat}} = (k_3)(k_5)(k_7)/(k_5)(k_7) + (k_3)(k_7) + (k_3)(k_5)$ and $K_M = k_{\text{cat}}\{(k_2 + k_3)/(k_1)(k_3)\}$. The theoretical steady-state kinetic constants are $k_{\text{cat}} = 58 \text{ s}^{-1}$ and $K_M = 39 \text{ }\mu\text{M}$. The theoretical values of k_{cat} and K_M are within a factor of 3 of the experimentally determined values at 2 °C: $k_{\text{cat}} = 130 \pm 30 \text{ s}^{-1}$ and $K_M = 90 \pm 50 \text{ }\mu\text{M}$.

RFQ–EPR Studies.

The EPR spectrum of Co^{II}-substituted ImiS is shown in Figure 6A and was simulated assuming a single paramagnetic species with $S = 3/2$, $M_S = |\pm 1/2\rangle$, $g_{x,y} = 2.25$, $g_z = 2.31$, and $E/D = 0.076$ (Figure 4B). No other Co^{II} species were detected between 4 and 13 K, and at microwave powers up to 40 mW, an $M_S = |\pm 3/2\rangle$ signal that was evident in some preparations of ImiS upon addition of substoichiometric Co^{II} (12) was not observed in the present work; this may be related to the higher pH employed (7.0 versus 6.5) and the known propensity of Co^{II} to adopt higher coordination numbers when possible (49). Upon the reaction of ImiS with imipenem for 10 ms, the spectrum (Figure 6C) had clearly changed and subtraction of the resting signal indicated the appearance of a rhombic signal (Figure 7A) for which only the two low-field resonances could be resolved. From the EPR spectrum after a 21 ms reaction time (Figure 6D), a second species (Figure 7B) could be clearly isolated by subtraction of the resting signal and was simulated (Figure 7C) using $S = 3/2$, $M_S = |\pm 1/2\rangle$, $g_{x,y} = 2.24$, $g_z = 2.18$, $E/D = 0.145$, and $A_{\nu}({}^{59}\text{Co}) = 40 \text{ G}$. It should be noted that, while the line shape was best-simulated including an unresolved hyperfine coupling on the lowest field feature (g_y for $M_S = |\pm 1/2\rangle$ of $S = 3/2$), the experimental data only suggested three barely resolved hyperfine lines and the data were not of sufficient signal-to-noise to confirm a full hyperfine pattern by the use of higher derivatives. The “21 ms” experimental spectrum (Figure 6D) was well-modeled by the addition of the simulations of the resting signal, accounting for 94% of the spins, and the rhombic signal, accounting for 6%. It is not clear whether the rhombic signal after 10 ms is the same as that after 21 ms; while the two lower field resonances clearly coincide, the high-field g_z resonance may be either broadened or shifted in the “10 ms” spectrum compared to the “21 ms” spectrum, perhaps indicating some very subtle structural differences. The EPR spectrum continued to change upon further reaction. The spectrum after 32 ms (Figure 6F) was again composed of the resting and rhombic signals (Figures 6G and 7D), and after 73 ms (Figure 6E), the intensity of the rhombic signal was greater than that after 21 ms by a factor of about 1.6, corresponding to 10% of the total Co^{II}. When rapid-freeze-quenched samples were thawed and refrozen after 2 s, an EPR signal (Figure 6I) consisting of a 35% resting signal and 65% of a third distinct signal, the “product” signal, was observed. The product signal was isolated (Figure 7F) by subtraction of the resting signal from Figure 6I and could be simulated (Figure 7G) assuming $S = 3/2$, $M_S = |\pm 1/2\rangle$, $g_{x,y} = 2.35$, $g_z = 2.12$, and $E/D = 0.13$. An enzyme-bound product signal was also observed in RFQ–EPR spectra of B3 MβL L1 (21).

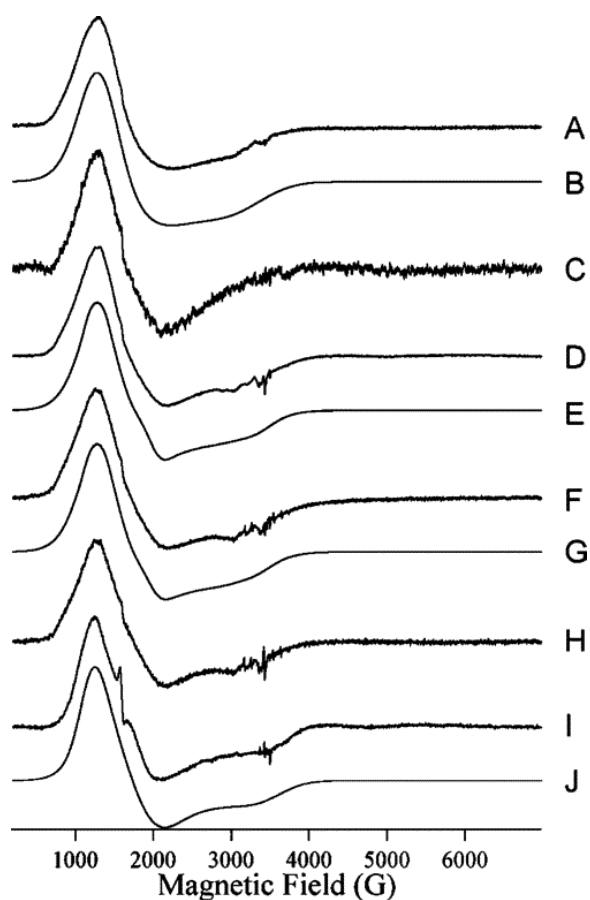


Figure 6 Trace A shows the resting EPR signal of Co^{II}-substituted ImiS. Initial concentrations of ImiS and imipenem were 1 and 5 mM, respectively. Traces C, D, F, H, and I show the EPR spectra of Co^{II}-substituted ImiS upon the reaction with imipenem for 10 ms at 2 °C (C), 21 ms at 2 °C (D), 32 ms at 2 °C (F), 73 ms at 2 °C (H), and 2 s at 2 °C (I). Trace B is a computer simulation of trace A, assuming $S = 3/2$, $M_S = |\pm 1/2\rangle$, $g_{x,y} = 2.25$, $g_z = 2.31$, and $E/D = 0.076$. Traces E, G, and J are models for D, F, and I, respectively, and consist of $(0.94 \times A) + (0.06 \times \text{trace C of Figure 7})$ (E), $(0.89 \times A) + (0.11 \times \text{trace C of Figure 7})$ (F), and $(0.45 \times A) + (0.65 \times \text{trace C of Figure 7})$ (I). Experimental EPR spectra were recorded at 12 K with 1 mW microwave power at 9.63 GHz. A 10 G (1 mT) field modulation at 100 kHz was employed.

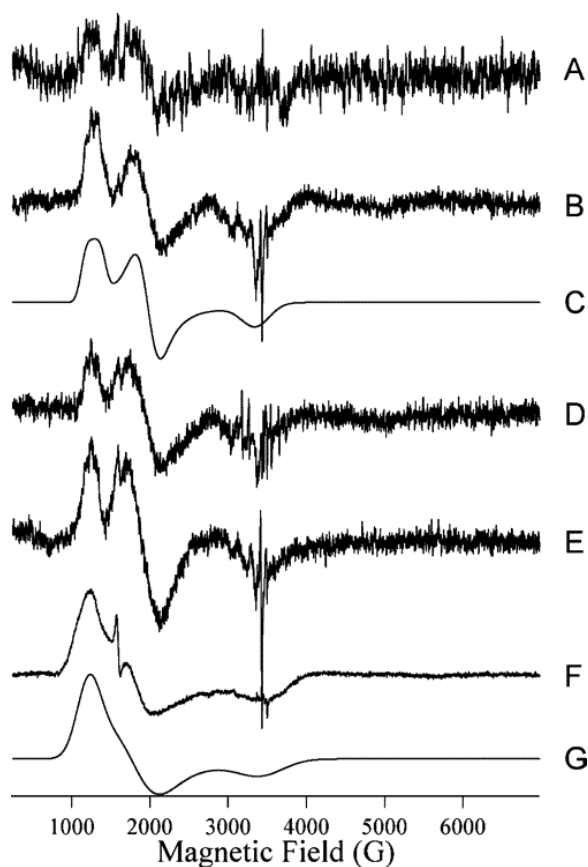


Figure 7 Isolated species. Traces A, B, D, E, and F are the EPR difference spectra generated by subtraction of the resting signal (trace A of Figure 6) from those of ImiS upon the reaction with imipenem at 2 °C for 10 ms, 21 ms, 32 ms, 73 ms, and 2 s, respectively. Traces C and G are the computer simulations of traces B and F, assuming $S = 3/2$, $M_S = |\pm 1/2\rangle$, $g_{x,y} = 2.24$, $g_z = 2.18$, $E/D = 0.145$, and $A_y(^{59}\text{Co}) = 40$ G and $S = 3/2$, $M_S = |\pm 1/2\rangle$, $g_{x,y} = 2.35$, $g_z = 2.12$, and $E/D = 0.13$.

Discussion

There have been many reports on the reaction mechanisms of dinuclear Zn^{II}-containing MβLs (from subgroups B1 and B3). In studies using CcrA and L1 and nitrocefin as the substrate, a ring-opened, nitrogen anionic intermediate was identified and kinetic studies revealed that the protonation of this intermediate was rate-limiting (17–20, 41). RFQ–EPR studies demonstrated that this intermediate yielded a novel EPR signal (21). A similar intermediate has not been observed in studies with *Bacillus cereus* β-lactamase II (50). Spencer and co-workers later extended mechanistic studies on L1 using other substrates such as cefaclor and meropenem (48). Kinetic analyses revealed that β-lactam bond cleavage is rate-limiting with these substrates, and these authors hypothesized that the intermediate observed when nitrocefin is used as a substrate is unique to nitrocefin and due to the highly conjugated, bis-nitro-substituted styryl substituent (48). Therefore, the reaction mechanisms of the B1 and B3 MβLs are becoming clearer. In contrast, there is little mechanistic information [except that inferred by a recent crystal structure on CphA (11) and that proposed on the basis of very recent computational studies on CphA (51, 52)] on any of the mononuclear Zn^{II}-containing B2 MβLs.

Many enzymes, including L1 (27), exhibit substrate inhibition at high substrate concentrations (29); however, the concentrations of substrate required to inhibit ImiS are relatively low (>200 μM). Analysis of the steady-state kinetic data demonstrates that the observed substrate inhibition in ImiS is uncompetitive (Figure 1), which indicates that the inhibitory substrate molecule binds to the ES (or species derived from the ES) complex. With

ImiS, it is possible that the substrate could bind with the β -lactam carbonyl or the β -lactam nitrogen coordinated to the metal ion, with one binding mode being the catalytically active mode and one mode describing an inhibited enzyme. The scenario would be expected to result in competitive substrate inhibition. It has been proposed for the B1 and B3 M β Ls that there is a loop that extends over the active site that may play a role in catalysis by “clamping down” and activating the substrate during catalysis (42, 53, 54). In the case of CphA (and presumably ImiS), there is an α helix (α 3) that is located where this loop is in other enzymes (11). It is possible that a second molecule of the substrate could bind to ES and prevent this α helix from “clamping down” on the substrate. Further studies are required to better understand substrate inhibition in ImiS.

Our first efforts to probe the mechanism used pH dependence and solvent isotope studies. As previously reported for L1 and CcrA (18, 28, 41), there are no apparent inflection points in the pH dependence plots. With L1 and CcrA, it was argued that the pK_a of the bridging solvent group was much lower than 5, as a result of bridging two divalent Zn^{II} ions. On the basis of extensive literature precedents on Zn^{II} hydrolases (55–60), it is possible that the Zn^{II} in ImiS in conjunction with Asp120 could generate a hydroxide that has a $pK_a < 5$. However, recent computational studies (52), along with predictions from the crystallographic studies (11), suggest that the nucleophile in CphA is not generated by Zn^{II} and that the nucleophile is generated by assistance of His118 and Asp120 (11) or solely by Asp120 (52). In addition, our RFQ–EPR studies suggest that there are only five ligands bound to the metal during catalysis, and these ligands are most likely three amino acid residues (Asp120, Cys221, and His263) and two points of attachment from the substrate (see below) (11). If in fact the reactive nucleophile is generated without the direct coordination to the metal ion, we hypothesize that both Asp120 and His118 participate in the generation of this nucleophile and that the pK_a of this solvent molecule is atypically low.

ImiS exhibited a solvent isotope effect that was very similar to that of dinuclear Zn^{II} -containing L1 and CcrA (28, 41); however, it is possible that there are >1 rate-significant protons in flight for ImiS. These data demonstrate that there is a rate-significant proton transfer in the reaction catalyzed by ImiS (30). Given that the rate-limiting step is most likely C–N bond cleavage (see below), one potentially important proton transfer could be to the ring nitrogen in the product. It is also possible that a proton transfer from the solvent molecule to generate the putative nucleophile could explain why multiple, rate-limiting proton transfers are possible with ImiS.

The roles of Lys224 and Asn233 were probed using site-directed mutagenesis. Several groups have demonstrated that Lys224 is involved in substrate binding to several of the dinuclear- Zn^{II} -containing M β Ls (28, 42, 43, 61–64). In fact, the recent structure of CphA bound to product suggests that Lys224 interacts with the 3' carboxylate on the substrate (11), and computational studies support a role of Lys224 in substrate binding (51). In contrast, our studies on the K224T mutant indicate that Lys224 is involved with catalysis, suggesting that the orientation of the 3' carboxylate is catalytically important. Crystallographic and computational studies suggested a role of the backbone amide of Asn233 in forming a hydrogen bond with the 3' carboxylate on the substrate (11, 51), and computational studies additionally suggested that the side-chain amide of Asn233 hydrogen bonds with the β -lactam carbonyl on the substrate (52). Our mutagenesis studies demonstrate that the side chain of Asn233 is not involved in substrate binding or catalysis, which supports the former prediction but not the latter.

Stopped-flow fluorescence and UV–vis studies were used next to probe the mechanism of ImiS. Stopped-flow fluorescence traces were similar in appearance to those of L1 (32, 48). The fluorescence properties of L1 are due to a single Trp (Trp37), which is located in close proximity to the dinuclear Zn^{II} site (22). It is likely that the fluorescence changes upon substrate binding to ImiS are also due to a single tryptophan, possibly Trp87, which lies near the putative substrate-binding site and within 10 Å of Zn^{II} in CphA (11). Stopped-flow fluorescence studies of 120 μ M ImiS with 100 μ M imipenem (or meropenem) resulted in a rapid decrease in fluorescence ($k_{obs} = 160 \text{ s}^{-1}$) and a relatively slow regain in fluorescence ($k_{obs} = 98 \text{ s}^{-1}$). Stopped-flow UV–vis studies, which

monitored the hydrolysis of the β -lactam bond in the substrate (48), showed a rapid decrease in absorbance that was best-fitted with a single-exponential equation yielding a $k_{\text{obs}} = 97 \text{ s}^{-1}$. As previously suggested for L1 (48), the regain of fluorescence because of substrate loss and the loss of absorbance are due to β -lactam hydrolysis in ImiS, and this step is probably the rate-determining step.

In an effort to offer a minimal kinetic mechanism that describes the data, global analyses and KINSIM were used to test several different kinetic mechanisms. The single-turnover data of ImiS were best-fitted/simulated using the kinetic mechanism and rate constants shown in Scheme 1 and Table 2, respectively. The minimal kinetic mechanism of ImiS shown in Scheme 1 is very similar to that of L1 (48) and suggests that the rate-limiting step is β -lactam hydrolysis. This mechanism also suggests the existence of a second ES complex (ES* in Scheme 1). The absence of ES* in our global analyses and KINSIM fits resulted in poor fits of the data.

EPR spectroscopy of ImiS upon the reaction with imipenem identified two new imipenem-dependent signals because of isolated Co^{II} . One, the rhombic signal, is indicative of a highly distorted geometry and suggestive of 5-fold coordination of Co^{II} . The partial resolution of ^{59}Co hyperfine coupling of 40 G ($4.3 \times 10^{-3} \text{ cm}^{-1}$) indicates a narrow intrinsic EPR line and is entirely consistent with such a structure, in which the rigid ligand environment necessary to constrain the distorted structure precludes large strains in g and/or the zero-field splitting parameters. From a structural basis, therefore, it is likely that the rhombic signal corresponds to either ES* or EI in the reaction proposed in Figure 8. In principle, the kinetic studies should provide further information as to which intermediate likely accumulates in sufficient amounts to be observed by EPR. In the case of ImiS, however, the situation is complicated by the substrate inhibition observed with imipenem. In the EPR experiment, the initial substrate concentration in the reaction mixture (after mixing) was 2.5 mM, and by extrapolation of Figure 1, the overall reaction rate may be expected to be of the order of 10% of that of the optimum rate. Uncompetitive inhibition, which best fits the data for ImiS and imipenem (Figure 1), implies further binding of imipenem to either ES, ES*, or EI, rather than a second, nonproductive mode of binding to the hitherto uncomplexed enzyme. Because the inhibition is not competitive, any molecule of imipenem to interact with the active site of ImiS will rapidly form ES and the imipenem pool will be initially depleted according to k_1 and k_2 and more slowly as fewer naked ImiS molecules are available. Because the enzyme and substrate are mixed in a 1:1 ratio and because k_1 is high and $K_i > K_m$, substrate inhibition will only be a factor during the mixing time, when local relative concentrations of imipenem may be higher than the equilibrium concentration. The mixing time is estimated to be ~ 1 ms. This is comparable with the optimum rate of formation of ES*, and thus, the rate of formation of ES* from ES is unlikely to be impeded by more than a factor of 2 or so if this is indeed the step inhibited by excess substrate. Thus, ES* formation is likely to be complete between 1 and 2 ms after mixing. The formation of EI is expected after a further 7 ms, i.e., after 8–9 ms, and the rhombic species observed after 10 ms is, therefore, assignable to the EI complex. While the simplest interpretation of the EPR spectra beyond 10 ms invoked a single species (the rhombic) in addition to the resting species, the kinetics suggest an alternative explanation, that g_z of the rhombic species is indeed unresolved, as in the signal isolated by the difference from the 10 ms reacted sample, and that the appearance of a resolved high-field feature in spectra recorded at longer reaction times is due to a contribution from the product species. While the EPR data are not of sufficient quality to differentiate these two explanations, the latter is entirely consistent with the kinetics, because the product complex would be expected to begin accumulating at around 18–19 ms. Thus, it is proposed that the rhombic species represents EI and the product species represents EP.

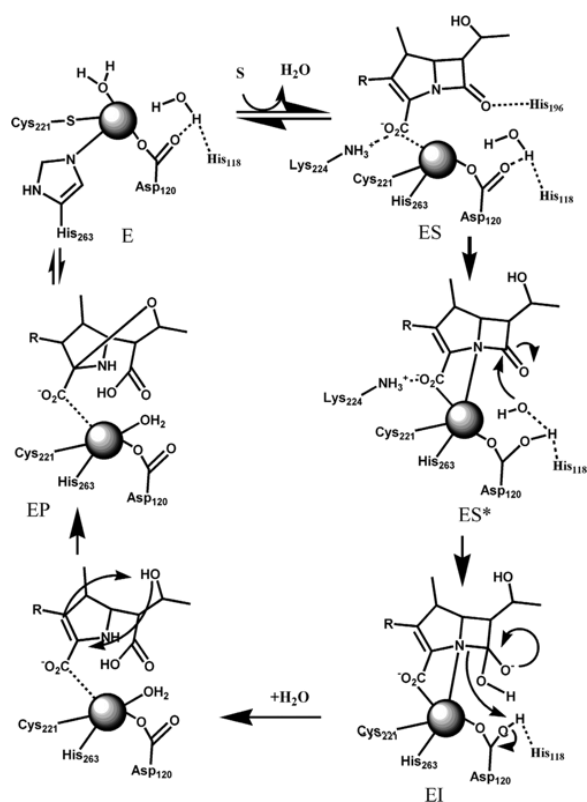


Figure 8 Proposed reaction mechanism for ImiS.

These data and previous crystallographic data (11) allow us to propose a reaction mechanism for ImiS (Figure 8). In the first step, the substrate binds to the active site replacing a water molecule. Initially, the carboxylate on the substrate interacts with Lys224 and Zn^{II}; however, on the basis of kinetic simulations, we believe that a second ES complex (labeled ES*) forms. We postulate that the Zn^{II}-substrate nitrogen interaction forms in ES*, generating a five-coordinate metal center. In our proposed mechanism, the nucleophile is generated by Asp120 and His118 as previously proposed (11); this nucleophile attacks the β -lactam carbonyl, possibly activated by His196 (11), to generate a tetrahedral intermediate, which we have labeled EI. It is important to note that the recent computational study suggested that a tetrahedral intermediate does not form in the proposed mechanism of CphA (52), and our data cannot support nor refute this hypothesis. It is entirely possible that EI is in fact a ring-opened, unprotonated species, similar to that reported in studies with CcrA and L1 when reacted with nitrocefin (17, 19, 21). In either case, a proton must be transferred to the ring-opened nitrogen to generate the product. We have also included the structure of the EP complex in the mechanism because this species was detected by RFQ-EPR studies. The inclusion of an EP complex in our kinetic simulations did not affect the fits as long as the rate of formation of EP is much faster than the breakdown of EI. Our spectroscopic data do not support the previous hypothesis (52) of Asp120 releasing from the metal ion during catalysis, yielding a four-coordinate intermediate.

The recent crystal structure of CphA showed the presence of a bicyclic product of biapenem in the active site of the enzyme (11). The authors proposed that, after β -lactam bond cleavage, a substantial bond rotation occurs that allows for the proton on the hydroxyethyl substituent found on all carbapenems to transfer to the 2' position on the five-membered ring of the substrate and for the nucleophilic attack of the oxygen at the 3 position. Because of steric constraints, it is clear that this cyclization occurs after C-N bond cleavage. Our product inhibition data strongly suggest that the bicyclic product is kinetically competent and is the final product of the reaction catalyzed by ImiS.


The results described herein demonstrate that MβLs from each of the distinct subclasses share a common rate-determining step, which is C–N bond cleavage. This fact suggests that inhibitors designed on this step will inhibit all MβLs, regardless of whether the enzymes are mono- or dinuclear Zn^{II}-containing enzymes.

Acknowledgment

The authors thank Professor Hua Guo of the University of New Mexico for helpful discussions, particularly those involving the timing of the formation of the bicyclic product.

References

- 1 Walsh, C. T., and Wright, G. D. (2005) Introduction: Antibiotic resistance, *Chem. Rev.*105, 391–393.
- 2 Neu, H. C. (1992) The crisis in antibiotic resistance, *Science*257, 1064–1073.
- 3 Heinz, U., and Adolph, H. W. (2004) Metallo-β-lactamases: Two binding sites for one catalytic metal ion? *Cell. Mol. Life Sci.*61, 2827–2839.
- 4 Walsh, T. R., Toleman, M. A., Poirel, L., and Nordmann, P. (2005) Metallo-β-lactamases: The quiet before the storm? *Clin. Microbiol. Rev.*18, 306–325.
- 5 Galleni, M., Lamotte-Brasseur, J., Rossolini, G. M., Spencer, J., Dideberg, O., and Frere, J. M. (2001) Standard numbering scheme for class B β-lactamases, *Antimicrob. Agents Chemother.*45, 660–663.
- 6 Garau, G., Garcia-Saez, I., Bebrone, C., Anne, C., Mercuri, P., Galleni, M., Frere, J. M., and Dideberg, O. (2004) Update of the standard numbering scheme for class B β-lactamases, *Antimicrob. Agents Chemother.*48, 2347–2349.
- 7 Valladares, M. H., Felici, A., Weber, G., Adolph, H. W., Zeppezauer, M., Rossolini, G. M., Amicosante, G., Frere, J. M., and Galleni, M. (1997) Zn(II) dependence of the *Aeromonas hydrophila* AE036 metallo-β-lactamase activity and stability, *Biochemistry*36, 11534–11541.
- 8 Janda, J. M., and Duffey, P. S. (1988) Mesophilic Aeromonads in human diseases: Current taxonomy, laboratory identification, and infectious disease spectrum, *Rev. Infect. Dis.*10, 980–987.
- 9 Jones, B. L., and Wilcox, M. H. (1995) Aeromonas infections and their treatment, *J. Antimicrob. Chemother.*35, 453–461.
- 10 Borrell, N., Figueras, M., and Guarro, J. (1998) Phenotypic identification of *Aeromonas* genomospecies from clinical and environmental sources, *Can. J. Microbiol.*44, 103–108.
- 11 Garau, G., Bebrone, C., Anne, C., Galleni, M., Frere, J. M., and Dideberg, O. (2005) A metallo-β-lactamase enzyme in action: Crystal structure of the monozinc carbapenemase CphA and its complex with biapenem, *J. Mol. Biol.*345, 785–795.
- 12 Crawford, P. A., Yang, K. W., Sharma, N., Bennett, B., and Crowder, M. W. (2005) Spectroscopic studies on cobalt(II)-substituted metallo-β-lactamase ImiS from *Aeromonas veronii* bv. *sobria*, *Biochemistry*44, 5168–5176.
- 13 Toney, J. H., and Moloughney, J. G. (2004) Metallo-β-lactamase inhibitors: Promise for the future? *Curr. Opin. Invest. Drugs*5, 823–826.
- 14 Siemann, S., Clarke, A. J., Viswanatha, T., and Dmitrienko, G. I. (2003) Thiols as classical and slow-binding inhibitors of IMP-1 and other binuclear metallo-β-lactamases, *Biochemistry*42, 1673–1683.
- 15 Heinz, U., Bauer, R., Wommer, S., Meyer-Klaucke, W., Papamichaels, C., Bateson, J., and Adolph, H. W. (2003) Coordination geometries of metal ions in d- or l-captopril-inhibited metallo-β-lactamases, *J. Biol. Chem.*278, 20659–20666.
- 16 Buynak, J. D., Chen, H., Vogeti, L., Gadhachanda, V. R., Buchanan, C. A., Palzkill, T., Shaw, R. W., Spencer, J., and Walsh, T. R. (2004) Penicillin-derived inhibitors that simultaneously target both metallo- and serine-β-lactamases, *Bioorg. Med. Chem. Lett.*14, 1299–1304.
- 17 McManus-Munoz, S., and Crowder, M. W. (1999) Kinetic mechanism of metallo-β-lactamase L1 from *Stenotrophomonas maltophilia*, *Biochemistry*38, 1547–1553.
- 18 Wang, Z., and Benkovic, S. J. (1998) Purification, characterization, and kinetic studies of soluble *Bacteroides fragilis* metallo-β-lactamase, *J. Biol. Chem.*273, 22402–22408.

- 19 Wang, Z., Fast, W., and Benkovic, S. J. (1998) Direct observation of an enzyme-bound intermediate in the catalytic cycle of the metallo- β -lactamase from *Bacteroides fragilis*, *J. Am. Chem. Soc.*120, 10788.
- 20 Wang, Z., Fast, W., and Benkovic, S. J. (1999) On the mechanism of the metallo- β -lactamase from *Bacteroides fragilis*, *Biochemistry*38, 10013–10023.
- 21 Garrity, J. D., Bennett, B., and Crowder, M. W. (2005) Direct evidence that reaction intermediate in metallo- β -lactamase is metal bound, *Biochemistry*44, 1078–1087.
- 22 Garrity, J. D., Pauff, J. M., and Crowder, M. W. (2004) Probing the dynamics of a mobile loop above the active site of L1, a metallo- β -lactamase from *Stenotrophomonas maltophilia*, via site-directed mutagenesis and stopped-flow fluorescence spectroscopy, *J. Biol. Chem.*279, 39663–39670.
- 23 Bounaga, S., Laws, A. P., Galleni, M., and Page, M. I. (1998) The mechanism of catalysis and the inhibition of the *Bacillus cereus* zinc-dependent β -lactamase, *Biochem. J.*331, 703–711.
- 24 Dal Peraro, M., Llarrull, L. I., Rothlisberger, U., Vila, A. J., and Carloni, P. (2004) Water-assisted reaction mechanism of monozinc β -lactamases, *J. Am. Chem. Soc.*126, 12661–12668.
- 25 Crawford, P. A., Sharma, N., Chandrasekar, S., Sigdel, T., Walsh, T. R., Spencer, J., and Crowder, M. W. (2004) Over-expression, purification, and characterization of metallo- β -lactamase ImiS from *Aeromonas veronii* *bv. sobria*, *Protein Expression Purif.*36, 272–279.
- 26 Webb, J. L. (1963) *Enzyme and Metabolic Inhibitors*, Vol. 1, Academic Press: New York.
- 27 Crowder, M. W., Walsh, T. R., Banovic, L., Pettit, M., and Spencer, J. (1998) Overexpression, purification, and characterization of the cloned metallo- β -lactamase L1 from *Stenotrophomonas maltophilia*, *Antimicrob. Agents Chemother.*42, 921–926.
- 28 Yanchak, M. P., Taylor, R. A., and Crowder, M. W. (2000) Mutational analysis of metallo- β -lactamase CcrA from *Bacteroides fragilis*, *Biochemistry*39, 11330–11339.
- 29 Cornish-Bowden, A. (1995) *Analysis of Enzyme Kinetic Data*, Oxford University Press: Oxford, U.K.
- 30 Venkatasubban, K. S., and Schowen, R. L. (1984) The proton inventory technique, *CRC Crit. Rev. Biochem.*17, 1–44.
- 31 Schowen, K. B. J. (1978) in *Transition States of Biochemical Processes* (Gandour, R. D., and Schowen, R. L., Eds.) pp 225–283, Plenum Press: New York.
- 32 Carenbauer, A. L., Garrity, J. A., Periyannan, G., Yates, R. B., and Crowder, M. W. (2002) Probing substrate binding to metallo- β -lactamase L1 from *Stenotrophomonas maltophilia* by using site-directed mutagenesis, *BMC Biochemistry*3, 4–10.
- 33 Lobley, A., and Wallace, B. A. (2001) Dichroweb: A website for the analysis of protein secondary structure from circular dichroism spectra, *Biophys. J.*80, 1570.
- 34 Lobley, A., Whitmore, L., and Wallace, B. A. (2002) DICHROWEB: An interactive website for the analysis of protein secondary structure from circular dichroism spectra, *Bioinformatics*18, 211–212.
- 35 Frieden, C. (1993) Numerical integration of rate equations by computer, *Trends Biochem. Sci.*18, 58–60.
- 36 Hanson, G. R., Gates, K. E., Noble, C. J., Mitchell, A., Benson, S., Griffin, M., and Burrage, K. (2003) in *EPR of Free Radicals in Solids: Trends in Methods and Applications* (Shiotani, M., and Lund, A., Eds.) pp 197–237, Kluwer Press: Dordrecht, The Netherlands.
- 37 Bennett, B. (2002) EPR of Co(II) as a structural and mechanistic probe of metalloprotein active sites: Characterization of an aminopeptidase, *Curr. Top. Biophys.*26, 49–57.
- 38 Bennett, B., and Holz, R. C. (1997) EPR studies on the mono- and dicobalt(II)-substituted forms of the aminopeptidase from *Aeromonas proteolytica*. Insight into the catalytic mechanism of dinuclear hydrolases, *J. [ACS Full Text ], [CAS], Google Scholaropen URL*
- 39 Bennett, B., and Holz, R. C. (1997) Spectroscopically distinct cobalt(II) sites in heterodimetallic forms of the aminopeptidase from *Aeromonas proteolytica*: Characterization of substrate binding, *Biochemistry*36, 9837–9846.
- 40 Fersht, A. (1985) *Enzyme Structure and Mechanism*, 2nd ed., W. H. Freeman and Co., New York.
- 41 Garrity, J. D., Carenbauer, A. L., Herron, L. R., and Crowder, M. W. (2004) Metal binding Asp-120 in metallo- β -lactamase L1 from *Stenotrophomonas maltophilia* plays a crucial role in catalysis, *J. Biol. Chem.*279, 920–927.

- 42 Ullah, J. H., Walsh, T. R., Taylor, I. A., Emery, D. C., Verma, C. S., Gamblin, S. J., and Spencer, J. (1998) The crystal structure of the L1 metallo- β -lactamase from *Stenotrophomonas maltophilia* at 1.7 Å resolution, *J. Mol. Biol.*284, 125–136.
- 43 Concha, N. O., Rasmussen, B. A., Bush, K., and Herzberg, O. (1996) Crystal structure of the wide-spectrum binuclear zinc β -lactamase from *Bacteroides fragilis*, *Structure*4, 823–836.
- 44 Bordo, D., and Argos, P. (1991) Suggestions for safe residue substitutions in site-directed mutagenesis, *J. Mol. Biol.*217, 721–729.
- 45 Walsh, T. R., Hall, L., Assinder, S. J., Nichols, W. W., Cartwright, S. J., MacGowan, A. P., and Bennett, P. M. (1994) Sequence analysis of the L1 metallo- β -lactamase from *Xanthomonas maltophilia*, *Biochim. Biophys. Acta*1218, 199–201.
- 46 Rossolini, G. M., Franceschini, N., Riccio, M. L., Mercuri, P. S., Perilli, M., Galleni, M., Frere, J. M., and Amicosante, G. (1998) Characterization and sequence of the *Chryseobacterium (Flavobacterium) meningosepticum* carbapenemase: A new molecular class B β -lactamase showing a broad substrate profile, *Biochem. J.*332, 145–152.
- 47 Bellais, S., Poirel, L., Leotard, S., Naas, T., and Nordmann, P. (2000) Genetic diversity of carbapenem-hydrolyzing metallo- β -lactamases from *Chryseobacterium (Flavobacterium) indologenes*, *Antimicrob. Agents Chemother.*44, 3028–3034.
- 48 Spencer, J., Clark, A. R., and Walsh, T. R. (2001) Novel mechanism of hydrolysis of therapeutic β -lactams by *Stenotrophomonas maltophilia* L1 metallo- β -lactamase, *J. Biol. Chem.*276, 33638–33644.
- 49 Kremer-Aach, A., Klau, W., Bell, R., Strerath, A., Wunderlich, H., and Mootz, D. (1997) Cobalt as a probe for zinc in metalloenzyme model compounds? A comparison of spectroscopic features and coordination geometry of four- and five-coordinate complexes, *Inorg. Chem.*36, 1552–1563.
- 50 Rasia, R. M., and Vila, A. J. (2003) Mechanistic study of the hydrolysis of nitrocefin mediated by *B. cereus* metallo- β -lactamase, *ARKIVOC*3, 507–516.
- 51 Xu, D., Zhou, Y., Xie, D., and Guo, H. (2005) Antibiotic binding to monozinc CphA β -lactamase from *Aeromonas hydrophila*: Quantum mechanical/molecular mechanical and density functional theory studies, *J. Med. Chem.*48, 6679–6689.
- 52 Xu, D., Xie, D., and Guo, H. (2006) Catalytic mechanism of class B2 metallo- β -lactamase, *J. Biol. Chem.*281, 8740–8747.
- 53 Huntley, J. J. A., Fast, W., Benkovic, S. J., Wright, P. E., and Dyson, H. J. (2003) Role of a solvent-exposed tryptophan in the recognition and binding of antibiotic substrates for a metallo- β -lactamase, *Protein Sci.*12, 1368–1375.
- 54 Scrofani, S. D. B., Chung, J., Huntley, J. J. A., Benkovic, S. J., Wright, P. E., and Dyson, H. J. (1999) NMR characterization of the metallo- β -lactamase from *Bacteroides fragilis* and its interaction with a tight-binding inhibitor: Role of an active-site loop, *Biochemistry*38, 14507–14514.
- 55 Auld, D. S. (1997) in *Metal Sites in Proteins and Models: Phosphatases, Lewis Acids, and Vanadium* (Hill, H. A. O., Sadler, P. J., and Thomson, A. J., Eds.) pp 29–50, Springer-Verlag: New York.
- 56 Bertini, I., Luchinat, C., and Scozzafava, A. (1980) The acid base equilibria of carbonic anhydrase, *Inorg. Chim. Acta*46, 85–89.
- 57 Bertini, I., and Luchinat, C. (1994) The reaction pathways of zinc enzymes and related biological catalysts, *Bioinorg. Chem.* 37–106.
- 58 Christianson, D. W., and Cox, J. D. (1999) Catalysis by metal-activated hydroxide in zinc and manganese metalloenzymes, *Annu. Rev. Biochem.*68, 33–57.
- 59 Denisov, V. P., Jonsson, B. H., and Halle, B. (1999) Dynamics of functional water in the active site of native carbonic anhydrase from ^{17}O magnetic relaxation dispersion, *J. Am. Chem. Soc.*121, 2327–2328.
- 60 Vallee, B. L., and Auld, D. S. (1990) Active-site zinc ligands and activated H_2O of zinc enzymes, *Proc. Natl. Acad. Sci. U.S.A.*87, 220–224.
- 61 Toney, J. H., Wu, J. K., Overbye, K. M., Thompson, C. M., and Pompliano, D. L. (1997) High-yield expression, purification, and characterization of active, soluble *Bacteroides fragilis* metallo- β -lactamase, CcrA, *Protein Expression Purif.*9, 355–362.

- 62** Spencer, J., Read, J., Sessions, R. B., Howell, S., Blackburn, G. M., and Gamblin, S. J. (2005) Antibiotic recognition by binuclear metallo- β -lactamases revealed by X-ray crystallography, *J. Am. Chem. Soc.* **127**, 14439–14444.
- 63** Park, H., Brothers, E. N., and Merz, K. M. (2005) Hybrid QM/MM and DFT investigations of the catalytic mechanism and inhibition of the dinuclear zinc metallo- β -lactamase CcrA from *Bacteroides fragilis*, *J. Am. Chem. Soc.* **127**, 4232–4241.
- 64** Suarez, D., Brothers, E. N., and Merz, K. M. (2002) Insights into the structure and dynamics of the dinuclear zinc β -lactamase site from *Bacteroides fragilis*, *Biochemistry* **41**, 6615–6630.
- 1** Abbreviations: CD, circular dichroism; EPR, electron paramagnetic resonance; IPTG, isopropyl- β -D-thiogalactopyranoside; LB, Luria–Bertani; LC–MS, liquid chromatography–mass spectrometry; M β L, metallo- β -lactamase; PAGE, polyacrylamide gel electrophoresis; RFQ, rapid freeze quench; SDS, sodium dodecyl sulfate; Tris, tris(hydroxymethyl)aminomethane.